Experimental evaluation of shear behavior of pultruded GFRP perforated connectors embedded in concrete

Xiong, Zhihua; Liu, Yuqing; Zuo, Yize; Xin, Haohui

DOI
10.1016/j.compstruct.2019.110938

Publication date
2019

Document Version
Final published version

Published in
Composite Structures

Citation (APA)
Xiong, Z., Liu, Y., Zuo, Y., & Xin, H. (2019). Experimental evaluation of shear behavior of pultruded GFRP perforated connectors embedded in concrete. *Composite Structures*, *222*, Article 110938. https://doi.org/10.1016/j.compstruct.2019.110938

Composite Structures 222 (2019) 110938

Contents lists available at ScienceDirect

Composite Structures

journal homepage: www.elsevier.com/locate/compstruct

Experimental evaluation of shear behavior of pultruded GFRP perforated connectors embedded in concrete

Zhihua Xiong[a], Yuqing Liu[a], Yize Zuo[b], Haohui Xin[a,c,*]

[a] Department of Bridge Engineering, Tongji University, Shanghai, China
[b] China State Construction Co. Ltd., Beijing, China
[c] Faculty of Civil Engineering and Geosciences, Delft University of Technology, Delft, the Netherlands

ARTICLE INFO

Keywords:
Pultruded GFRP profiles
Shear connector
Pull-out tests
Strength equation

ABSTRACT

This paper presents experimental and analytical studies on the shear behavior of GFRP perforated connectors (GPC) embedded in concrete. A series of 26 pultruded GPC specimens were fabricated and tested under pull-out load. The experimental variables included the effects of plate thickness, plate hole's radius and penetrating rebars. Concrete dowel failure and GFRP shear-out failure were the two main failure patterns of GPC specimens. GFRP failure occurred in specimens with a thin plate, and ultimate strength is mainly affected by the hole's radius. The specimens with concrete dowel failure presented more ductile than the specimens with GFRP shear-out failure. The shear stiffness of GPC was determined based on load-slip curves. Finally, the ultimate strength equations of GPC incorporating the stress concentration in the GFRP plate and the restraint effect of penetrating rebar were proposed based on the test results. Good agreement between experimental and theoretical results was achieved. A critical thickness of GPC plate was proposed to guarantee sufficient strength and ductility.

1. Introduction

Glass fiber reinforced polymers (GFRP) have been widely used in various infrastructure projects in terms of relatively lower costs, high strength-to-weight ratio and corrosion resistance [1,2]. Typical applications in the bridge engineering of pultruded GFRP materials include bridge decks and girders. The bridge deck generally included GFRP-concrete composite deck [3–6] and all-GFRP bridge deck [7–10]. GFRP-concrete composite deck exploits the material merits of both concrete and GFRP, the deck itself could be used as stay-in-place formwork, and is one of the most important application types.

The prerequisite for GFRP-concrete composite deck to fulfill its load transfer function is completely connection between GFRP and concrete. As so far, bonded joints and mechanical connectors have been reported as common connection types between GFRP and concrete [11]. Epoxies are the most commonly employed adhesive for bonded connection in GFRP-concrete hybrid structure [12]. Sand-coated GFRP has been usually applied to increase the adhesive bonding between the concrete and GFRP member [13–15]. The strength of bonded connection has been largely determined by the chemical substances of the adhesion, including surface pre-treatment, long warming and curing process [14]. Mechanical connections generally include bolted joints [11], stud joints [11] and perforated connector [5].

Perforated connector has been widely adopted in steel-concrete composite structures [16,17]. The shear resistance of perforated connector comes from the interaction between the concrete dowel and the plate's hole. The shear strength of perforated connector could be affected by many factors, including the plate hole's radius, the thickness of the plate and penetrating rebars. In terms of GFRP perforated connectors (GPC) embedded in concrete, a strength equation was proposed by Cho et al. [18] based on the discrete spring model. Zou et al. [19] proposed the strength equations of GPC based on the work of Oguejiofor and Hosain [20]. Push-out tests is an alternative method to determine the shear behavior of GPC. While, push-out tests easily generate secondary bending moments due to the low elastic modulus of GFRP material, making the specimens under combined shear and bending load. The effect of penetrating rebars to the ultimate strength is also not considered in the earlier published studies. While it is reported in the literature [21] that penetrating rebars have huge effects on the failure mode of the concrete dowel, and it is necessary to investigate the penetrating rebars effects on the ultimate strength and typical failure mode. In addition, the shear stiffness of GPC is a commonly-used parameter during design of GFRP-concrete composite structures. Thus, it is important to evaluate the shear stiffness and shear strength of GPC through pull-out tests.

This paper presents a series of pull-out tests of GPC used in GFRP-

* Corresponding author at: Department of Bridge Engineering, Tongji University, Shanghai, China.
E-mail address: H.Xin@tudelft.nl (H. Xin).

https://doi.org/10.1016/j.compstruct.2019.110938
Received 3 February 2019; Received in revised form 11 April 2019; Accepted 2 May 2019
Available online 03 May 2019

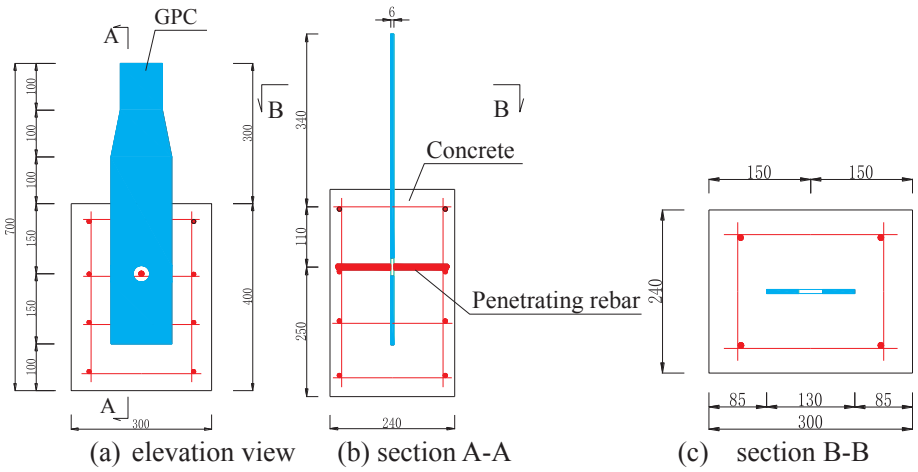

Fig. 1. Dimensions of GPC specimens (units: mm).

concrete composite deck. A total of 26 specimens were fabricated and tested, which involved the following parameters: the thickness of the pultruded plate, the radius of plate holes, the presence and the type of penetrating rebars. The shear stiffness of GPC was obtained by test data analysis. Moreover, the strength equations of GPC were proposed based on the test results in terms of failure modes. The proposed equations were validated by different experimental results. The critical thickness of GPC located on the border between GFRP shear failure and concrete dowel failure was adopted to avoid brittle failure.

2. Experimental program

2.1. Specimen fabrication

As shown in Fig. 1, GPC plates were cut by water-jet saw form stay-in-place formwork reported in [5]. It is noted that the gripped end was tapered to 90 mm while the width embedded in concrete was 130 mm to meet the width demand of the grip. To consider the deck's web joint assembling two separated deck part together, the double-plates specimens were fabricated and fastened by bolt and epoxy adhesion as shown in Fig. 2.

GPC plates were pre-installed in the wood formwork as shown in Fig. 3 and were lubricated to reduce the friction with concrete. After the deployment of the strain gauges, the concrete was casted, as shown in Fig. 3-c. The geometric and other parameters of all the pull-out specimens are listed in Table 1, in which the group denoted as “R” represents the radius of plate’s hole, “d” denotes the diameter of rebar, “G” denotes GFRP penetrating rebar and “D” denotes double-plates.

2.2. Material properties

The pultruded GFRP lamination was made up of 7 layers, in which reinforcement were E-glass roving, woven fabrics. The matrix was epoxy resin. The stacking sequence is shown in Fig. 4, with four types of laminas: (1) rovings for 0°-lamina; (2) unidirectional fabrics for the 90°-lamina; (3) woven fabrics for the ± 45° lamina and (4) chopped fabric

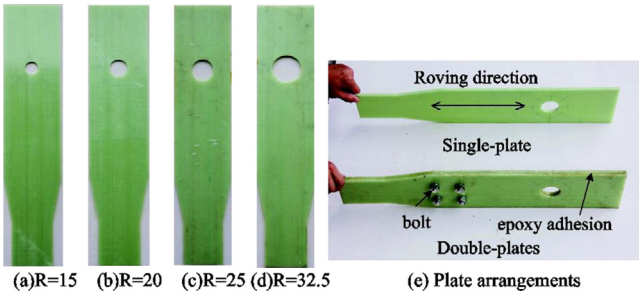

Fig. 2. Various plate hole’s radius and plate arrangements (units: mm).

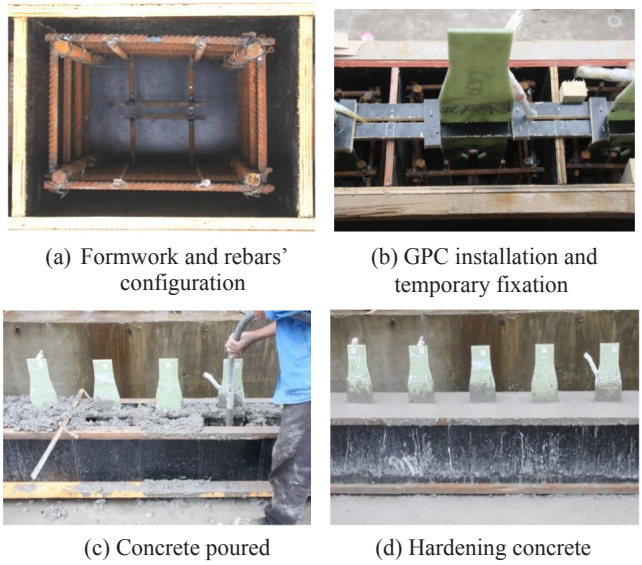

Fig. 3. Specimens fabrication.

Table 1
Details of GPC specimens.

Specimens No.	Plate arrangement	Plate hole’s radius R (mm)	Penetrating rebar’s diameter d_s (mm)	Rebar’s type	Thickness t (mm)
R15	Single-plate	30	–	Steel rebar	6
R20		40	–		
R25		50	–		
R15d10		30	10		
R20d10		40	10		
R20d16		40	16		
R25d10		50	10		
R25d16		50	16		
R25dG16		50	16	GFRP rebar	
R25d20		50	20	Steel rebar	
R32.5d20		65	20		
R20d16D	Double-plates	40	16		12
R25d16D		50	16		12

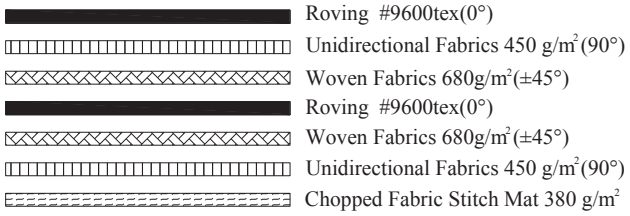

Fig. 4. Stacking sequences of pultruded GFRP plate.

Table 2
Material characteristics of pultruded GFRP profile.

Property	Value	Unit	Standard deviation
Longitudinal tensile strength	430.0	MPa	31.3
Longitudinal tensile modulus	45.5	GPa	4.5
Longitudinal compressive strength	491.4	MPa	54.7
Transverse tensile strength	67.6	MPa	2.8
Transverse tensile modulus	21.7	GPa	1.9
Transverse compressive strength	166.7	MPa	16.9
shear strength	58.4	MPa	10.1
shear modulus	9.8	GPa	0.9

Table 3
Mechanical properties of concrete.

Concrete cubes and average	Elastic modulus (MPa)	Compressive strength (MPa)
Cube1	3.75×10^4	47.3
Cube2	3.94×10^4	51.6
Cube3	3.49×10^4	53.8
Average	3.74×10^4	50.9

mats. All angles are relative to the pultrusion direction. The material characteristics of pultruded GFRP laminations were obtained by the coupon tests and summarized in Table 2 [5].

Three 150 mm-edge concrete cubes for compression test were poured and cured with moisture for 28 days. The material properties of concrete were tested in accordance with GB50010-2010 standard procedures [22] and a summary of experimental results are listed in Table 3. In addition, the properties of GFRP and steel rebars provided by the material manufacturer are summarized in Table 4.

2.3. Test setup

A set-up is designed for the pull-out tests, as shown in Fig. 5. This set-up was made up of two rigid plates, four Φ24 mm bolt shanks and a pinned bar. The specimens were fixed in the clamping frame and the tapered end of GFRP plates was gripped by the bottom clip. The pinned bar of the clamping frame was gripped by the top clip and pulled by the actuator, with a loading rate 1 mm/min and a capacity of ± 500 kN. Before the test, a preloading was applied in a ratio of 10% peak load to check the operation of the gauges demonstrated in Fig. 6 and the test rig. Two LVDTs (Linear Variable Differential Transducer) were set on the bottom of the clamping frame, one end is fixed on the concrete and

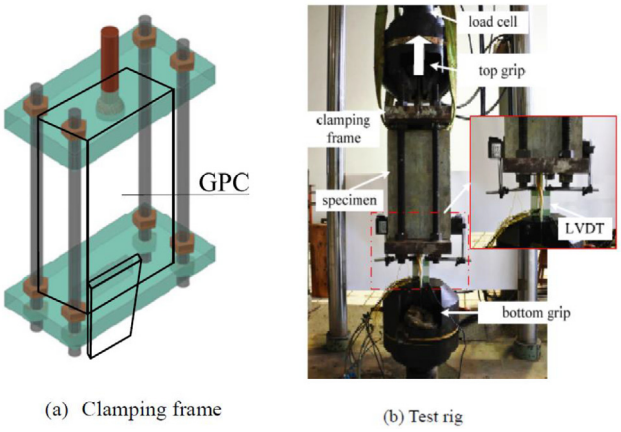

Fig. 5. Test setup.

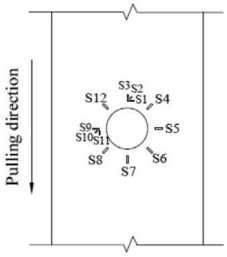

Fig. 6. Strain gauges.

the other end is fixed on the GFRP plate to record the slip.

3. Test results

3.1. Strain distribution

3.1.1. Strain distribution around the plate's hole

Selected strain data versus the ultimate shear strength of GFRP plate's hole are plotted in Fig. 7. Along the pulling direction, the strain at position S7 was in tension, while the strains at positions S3 and S4 were in compression. The strain around the hole ascended slowly in linear until the load reached $0.4V_u$. When the load is larger than $0.4V_u$, the compression strain accumulated rapidly. While the tensile strains around the hole remain its linear development.

3.1.2. Strain distribution of penetrating rebar

The strain of penetrating rebars versus ultimate shear strength is presented in Fig. 8. In the loading stage of 0–$0.4V_u$, the rebar's strain was very small. When the load increased from $0.4V_u$ to $0.7V_u$, the shear force gradually transmitted from concrete to rebar, and the rebar's strain developed rapidly. When the load increased near the peak, the rebar of the single-plate was still in elastic while the rebar's strain of the double-plates was beyond the yielding. For the specimen with GFRP penetrating rebar (R25dG16), the maximum strain was 1000 με, which is less than the ultimate strain 17,600 με.

Table 4
Mechanical properties of rebars.

Type of rebar	Diameter (mm)	Elastic modulus (MPa)	Yield strength (MPa)	Tensile strength (MPa)
Steel rebar	10	2.03×10^5 (SD*:9.65)	472.3 (SD:10.43)	676.0 (SD:13.89)
	16	2.05×10^5 (SD:10.29)	430.4 (SD:11.61)	648.1 (SD:9.36)
	20	2.03×10^5 (SD:9.52)	490.6 (SD:8.22)	655.8 (SD:9.15)
GFRP rebar	16	4.1×10^4	/	724.0

*Note: SD-Standard deviation.

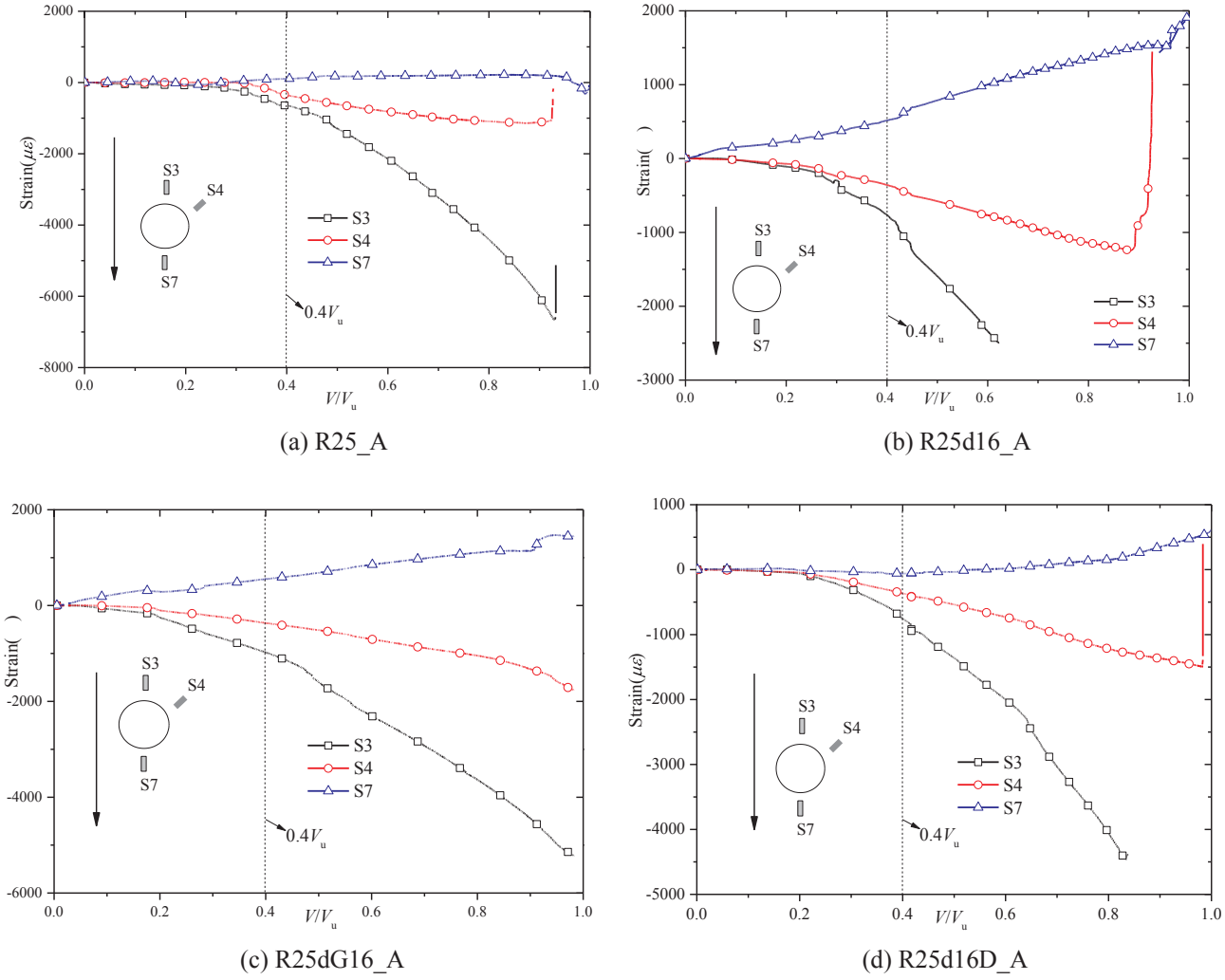

Fig. 7. Strain distribution around the plate's hole.

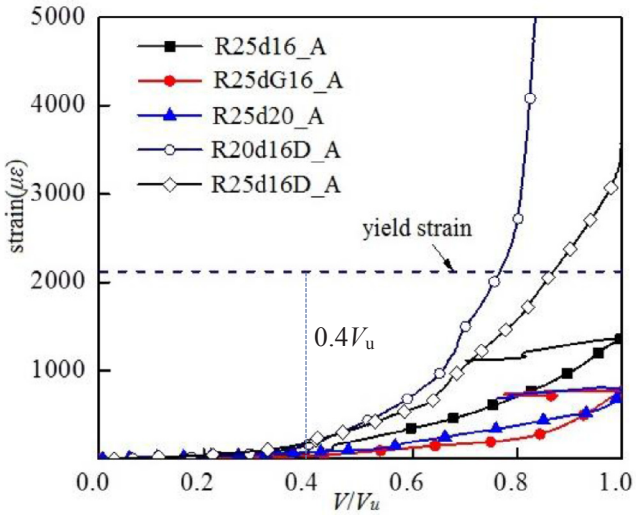

Fig. 8. Penetrating rebar's strain versus load curves.

3.2. Failure modes

The failure modes of GPC specimens are shown in Figs. 9 and 10 via cutting the specimens along the interface between GFRP and concrete. Two typical failure modes were observed, namely 1) shear-out failure of GFRP plate, 2) concrete dowel failure. In terms of double-plates specimens, the initial damage was due to the failure of concrete dowel, after then plate's hole was compressed and shear tearing failure (Fig. 10-a) occurred with the increasing of the interface slip. As shown in Fig. 10-b, the rebar was bended for the specimens with double-plates while relatively smaller plastic deformation was observed for the specimens with the single plate. As the hole's radius decreased and shear resistance increased, bending deformation of the rebar increased at the same slip. It is noted that shear resistance of GFRP lamination with hole plays a critical role for the single plate specimen, while the initial failure shifts from the plate's shear-out failure to concrete dowel failure when the lamination thickness is doubled. Since the concrete dowel holds the pressure and transfers it to the rebar and the plate, it reaches its compressive strength and fails first. As the crack develops, the rebar holds the force from the smashed concrete and then transfers to the plate.

Concrete's cracks of pull-out tests with double plates are displayed in Fig. 11. The first visual crack generally initiated from the center of the plate's hole and gradually extended to the side of the concrete block. With the load increasing, the crack developed to the top of the block and inclined crack emerged.

3.3. Load-slip curves

The slip displacement is obtained as the average values of the two LVDTs. A total of 26 specimens load-slip (LS) curves are listed in

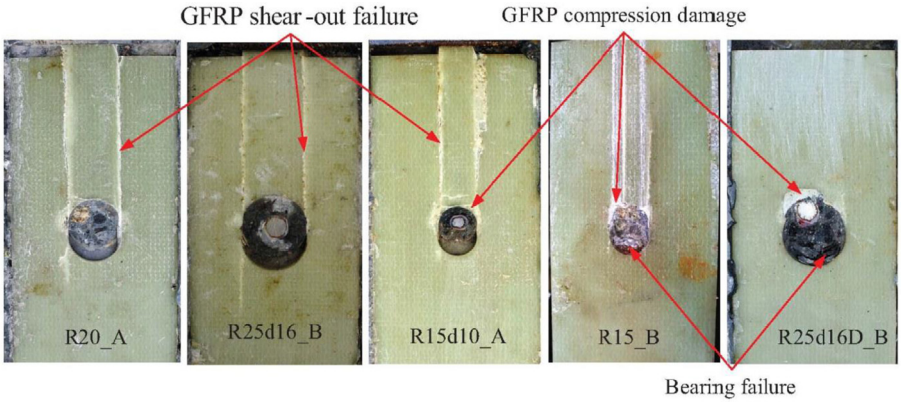

Fig. 9. Cut section of failed GPC specimens.

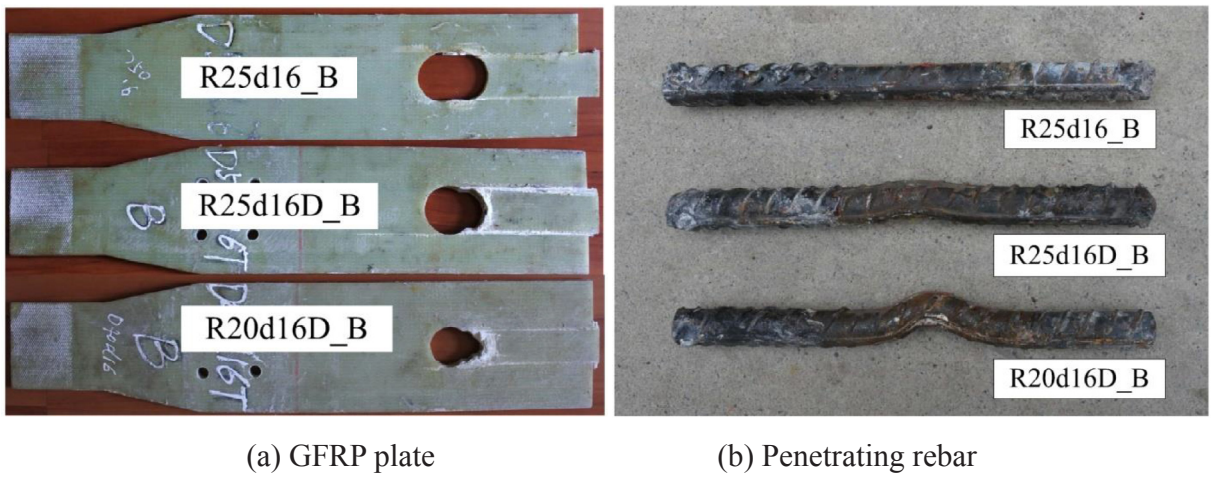

Fig. 10. Failure pattern's comparison of GPC specimens.

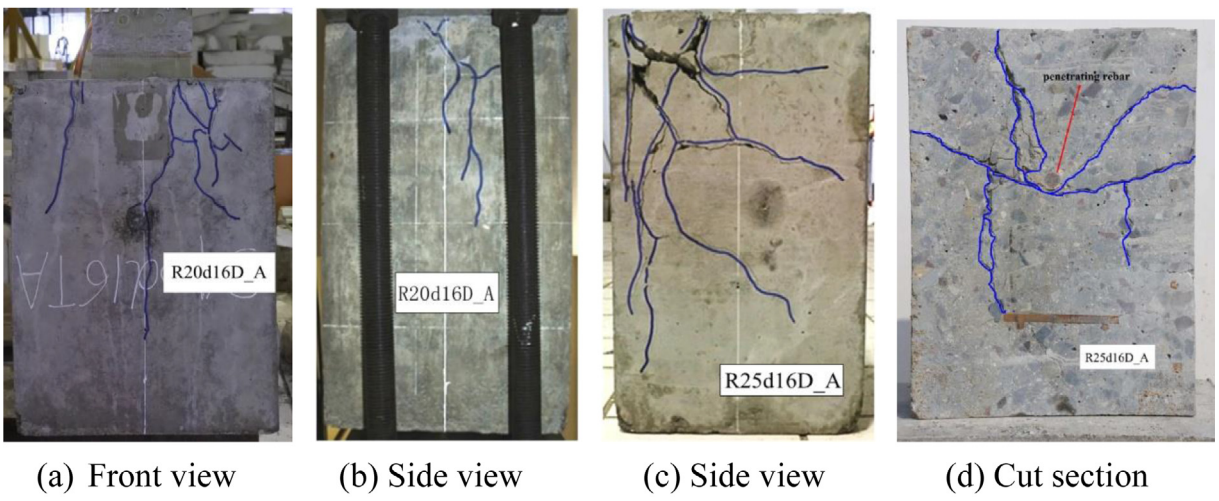

Fig. 11. Concrete crack.

Fig. 12. Three stages could be identified from LS curves, including elastic stage, plastic stage and failure stage. The detail is explained as follows:

1) In the elastic stage as shown in Fig. 13, the slip was relatively small when the load was less than $0.4V_u$. The load increased linearly with the development of slip. The development of the curve was similar to the result of Oehlers and Coughlan [23] on the research of shear studs. Thus, the shear stiffness is defined as the secant slope at the point $0.4V_u$. In order to validate this methodology, results were obtained for a load of $0.3V_u$ and the corresponding slip value. In the meantime, the slip calculated by the stiffness at $0.3V_u$ was compared to the measured value listed in Table 5. According to the deviation $\delta_{0.3vu}/\delta_{k,0.3vu}$ in Table 5, the $0.4V_u$ definition of stiffness showed a good representation of the elastic stage.
2) In the plastic stage, the relationship between shear load and the slip

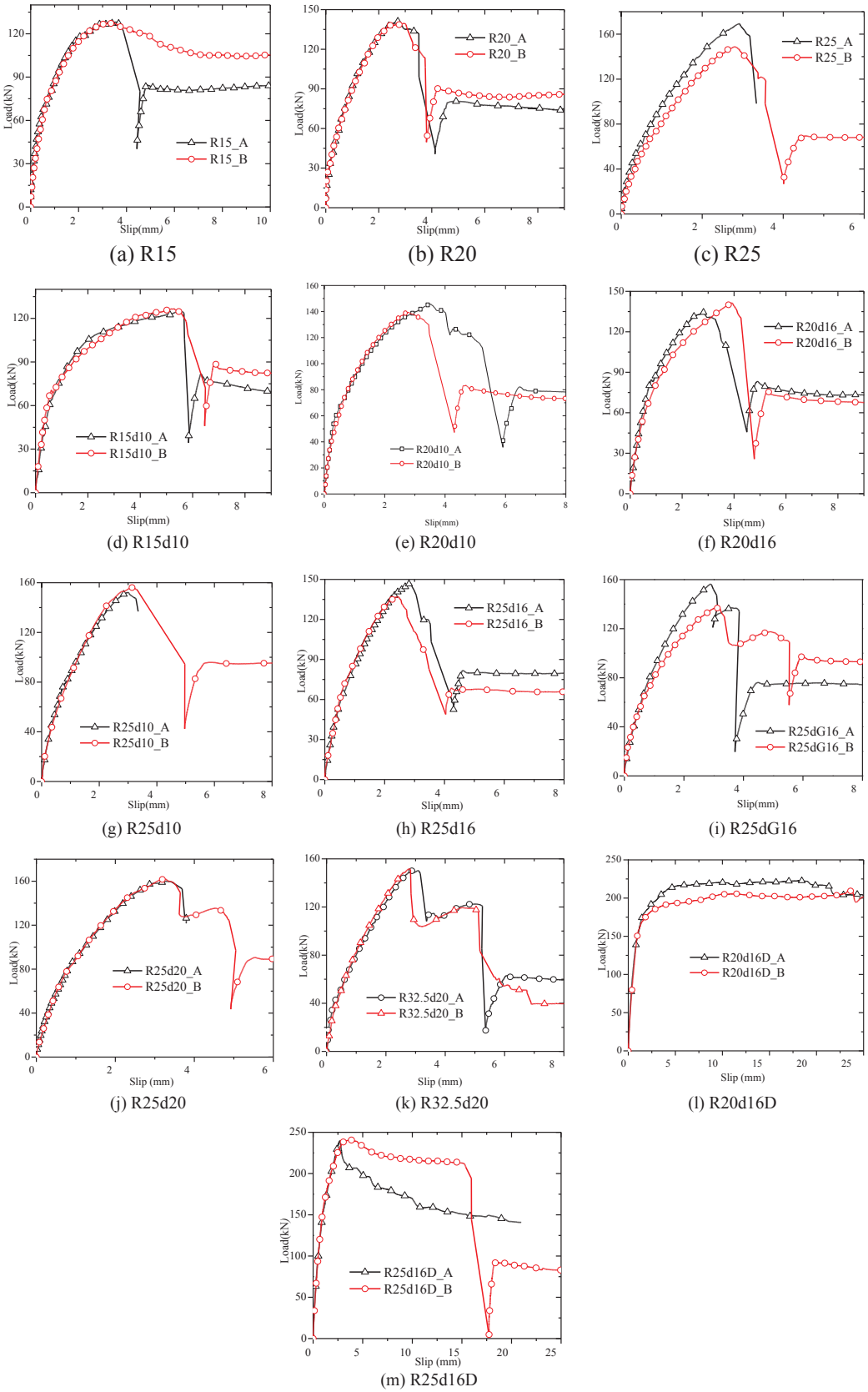

Fig. 12. LS curves of specimens.

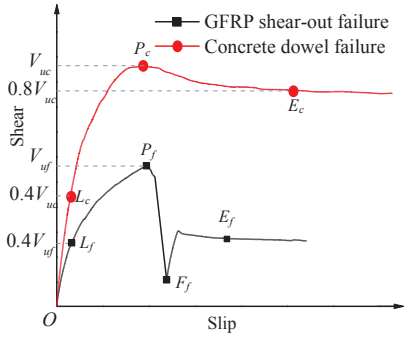

Fig. 13. LS curve generalization and its corresponding three stages.

Table 5
GPC's stiffness verification.

Specimens	$0.3V_u$ (kN)	Measured slip $\delta_{0.3vu}$ (mm)	Stiffness $k_{0.4vu}$ (kN/mm)	Calculated slip $\delta_{k,0.3vu}$ (mm)	$\delta_{0.3vu}/\delta_{k,0.3vu}$
R15_A	38.49	0.19	172.9	0.22	0.85
R15_B	38.28	0.25	134.1	0.29	0.88
R20_A	42.39	0.3	134.1	0.32	0.95
R20_B	41.88	0.25	128.9	0.32	0.77
R25_A	50.82	0.41	119.5	0.43	0.96
R25_B	44.61	0.38	98.6	0.45	0.84
R15d10_A	37.44	0.28	121.7	0.31	0.91
R15d10_B	37.98	0.25	144.1	0.26	0.95
R20d10_A	43.71	0.25	164.9	0.27	0.94
R20d10-B	41.85	0.25	121.3	0.35	0.72
R20d16_A	40.35	0.29	129.6	0.31	0.93
R20d16_B	42.42	0.34	111.8	0.38	0.90
R25d10_A	45.69	0.35	110.3	0.41	0.84
R25d10_B	46.86	0.39	102.7	0.46	0.85
R25d16_A	44.16	0.36	111.9	0.39	0.91
R25d16_B	41.13	0.33	122.5	0.34	0.98
R25dG16_A	46.89	0.4	105.8	0.44	0.90
R25dG16_B	41.16	0.32	108.3	0.38	0.84
R25d20_A	48.57	0.38	109.8	0.44	0.86
R25d20_B	47.94	0.39	112.9	0.42	0.92
R32.5d20_A	45.09	0.36	98.1	0.46	0.78
R32.5d20_B	45.51	0.42	97.6	0.47	0.90
R20d16D_A	66.87	0.26	227.7	0.29	0.89
R20d16D_B	62.94	0.28	153.9	0.41	0.68
R25d16D_A	71.94	0.31	201.1	0.36	0.87
R25d16D_B	72.3	0.34	199.2	0.36	0.94

turned out to be non-linear. As the slip ascended, the load increment became flat till the peak load.

3) In the failure stage, the load-slip curves seriously depended on failure modes. For the concrete dowel failure, the load descended slowly after the peak load and the specimens were ductile. For the GFRP shear-out failure, it showed brittle characteristics that once reaching the peak load it suddenly dropped to a fair low point and then rise to the point E, as shown in Fig. 13. This phenomenon was attributed to the brittle nature of GFRP material.

All the 26 specimens' ultimate strength and stiffness are summarized in Table 6. The stiffness of GPC was defined as $0.4V_u/\delta_{0.4vu}$ due to its verification in Table 5.

4. Parameters affecting failure mechanisms

4.1. Effects of perforated plate thickness

The effects of perforated plate thickness are shown in Fig. 14-a for the 25 mm hole radius case. The related pull-out specimens are R25d16 and R25d16D, in which R25d16 is single-plate and companion R25d16D is double-plate. Observed from Fig. 14(a), the ultimate strength of the single-plate and double-plate are 137.1 kN and 241.0 kN respectively. The ultimate strength of double-plate specimens is improved 75.8% than that of single-plate. The single-plate specimens' failure mode is the shear-out failure. By increasing the thickness of the perforated plate, the failure mode becomes concrete dowel failure due to larger shear resistance. As a result, the ultimate strength and stiffness are both improved by increasing the thickness.

Table 6
Pull-out test data.

Specimens	Stiffness $k_{0.4vu}$ (kN/mm)		Ultimate strength V_u (kN)		Slip δ_u (mm)		Failure pattern*
	test	average	test	average	test	average	
R15_A	172.9	153.5	128.3	128.0	3.55	3.52	GF
R15_B	134.1		127.6		3.49		CF
R20_A	134.1	131.5	141.3	140.5	2.74	2.855	GF
R20_B	128.9		139.6		2.97		GF
R25_A	119.5	109.1	169.4	159.1	2.92	2.875	GF
R25_B	98.6		148.7		2.83		GF
R15d10_A	121.7	132.9	124.8	125.7	5.59	5.39	GF
R15d10_B	144.1		126.6		5.19		GF
R20d10_A	164.9	143.1	145.7	142.6	3.49	3.14	GF
R20d10-B	121.3		139.5		2.79		GF
R20d16_A	129.6	120.7	134.5	138.0	2.84	3.375	GF
R20d16_B	111.8		141.4		3.91		GF
R25d10_A	110.3	106.5	152.3	154.3	3.00	3.075	GF
R25d10_B	102.7		156.2		3.15		GF
R25d16_A	111.9	117.2	147.2	142.2	2.85	2.65	GF
R25d16_B	122.5		137.1		2.45		GF
R25dG16_A	105.8	107.1	156.3	146.8	2.90	3.025	GF
R25dG16_B	108.3		137.2		3.15		GF
R25d20_A	109.8	111.4	161.9	160.9	2.78	3.025	GF
R25d20_B	112.9		159.8		3.27		GF
R32.5d20_A	98.1	97.9	150.3	151.0	2.88	2.845	GF
R32.5d20_B	97.6		151.7		2.81		GF
R20d16D_A	227.7	190.8	222.9	216.4	18.04	20.9	CF
R20d16D_B	153.9		209.8		23.76		CF
R25d16D_A	201.1	200.2	239.8	240.4	2.71	3.19	CF
R25d16D_B	199.2		241.0		3.67		CF

*Note: GF-GFRP shear-out failure, CF-Concrete dowel failure.

4.2. Effects of plate hole radius

The effects of plate hole radius are shown in Fig. 14-b and -c in terms of different failure modes. The radius is subdivided as 15 mm, 20 mm and 25 mm. It is found that the various radius makes a significant influence on ultimate strength.

For the specimens with GFRP shear-out failure, when the radius increases from 15 mm to 20 mm, the ultimate strength is improved 9.8% and the slip decreases 18.9%. When the radius increases from 20 mm to 25 mm, the ultimate strength is improved 13.2% and the slip increases 0.7%. However, as the radius increases from 25 mm to 32.5 mm, the ultimate strength decreases 5.3% and the slip increases 3.3%. The ultimate strength of specimens increases originally and decreases afterward as the hole's radius ascends. The slip decreases considerably as the hole's radius ascends. The ultimate strength is determined by a balance between shear behavior of GFRP plate and the increasing contact area of the concrete dowel.

In terms of the specimen whose failure pattern is concrete dowel failure, the various radius makes a substantial effect on the ultimate strength and stiffness. The ultimate strength is improved by 11.1% as the radius increases from 20 mm to 25 mm, and shear stiffness is slightly improved by 4.9%. This could be attributed to the increased radius which elevates the bearing area of the concrete dowel.

4.3. Effect of penetrating rebars

As discussed in Section 3.3, in respect of the specimens which

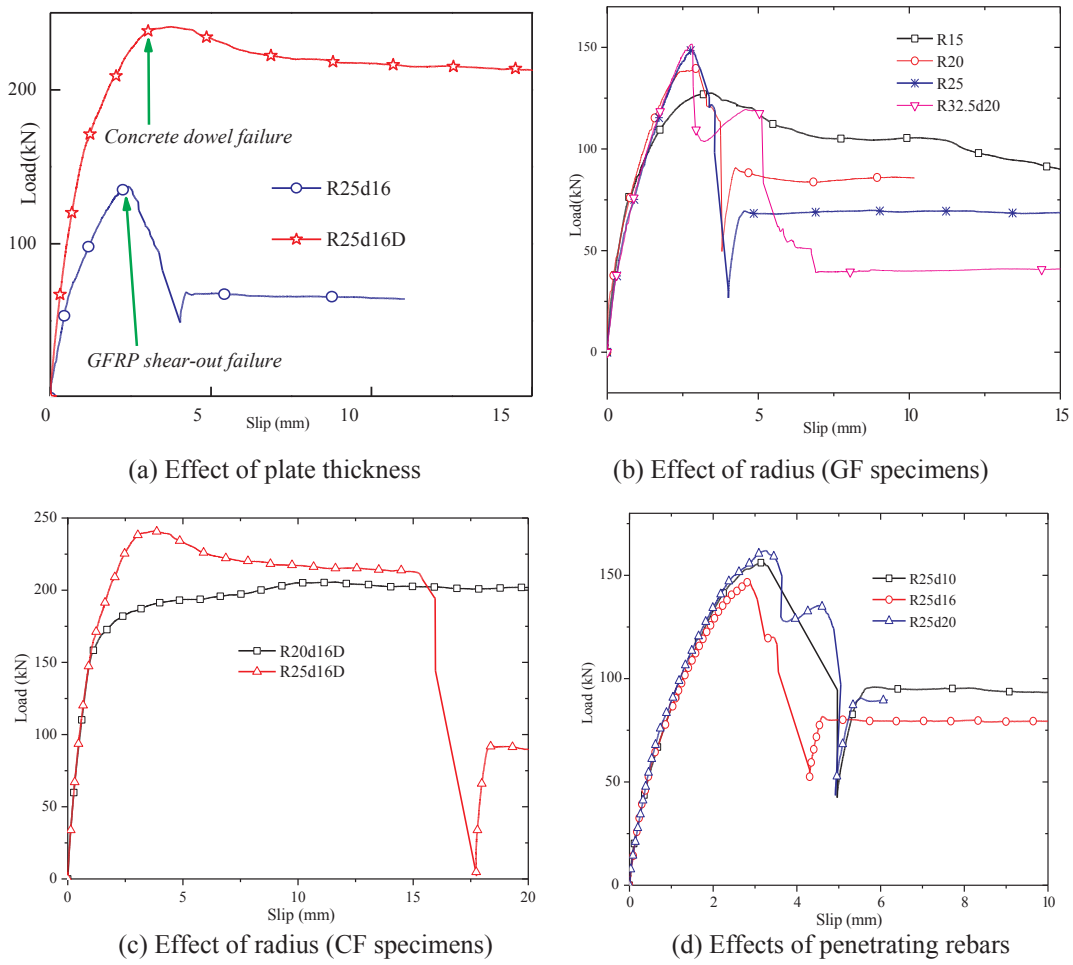

Fig. 14. Parameters' effect on GPC's performance.

conforms to the concrete dowel failure mode, the rebar plays a critical role in the shear force transfer.

For the specimens which fail due to shear-out of GFRP lamination, the ultimate strength of specimens with 10 mm diameter penetrating rebar is only 1.5% larger than that without penetrating rebar. When the penetrating rebar's diameter increases from 10 mm to 16 mm, the ultimate strength descends 7.8% and the stiffness increases 10% respectively. When the penetrating rebar's diameter increases from 16 mm to 20 mm, the ultimate strength increases 13.1% and the stiffness descends 4.9%. It appears that the correlation between the performance of GPC and the penetrating rebar is not obvious.

4.4. Failure mechanism

As generalized in Section 3.3, when the load is less than $0.4V_u$, the curve ascends in linear. As the load exceeds $0.4V_u$, the curve goes into the nonlinear growth stage. In according to the obtained test data, the force transfer of the GPC could be generalized as: in the elastic stage ($0.4V_u$), the concrete dowel provides the shear resistance, and the slip is mainly due to relative deformation between the concrete dowel and GFRP plate. In the plastic stage ($0.4V_u$), for the pull-out specimens with small thickness, the plate has a small shear area and presents shear-out failure, as illustrated in Fig. 15(a). For the pull-out specimens with large thickness, concrete dowel plays a key role in the shear resistance and crushes at the ultimate state, as illustrated in Fig. 15(b). The slip is generated by the relative deformation of concrete dowel, rebar and GFRP plate. In the failure stage, the pull-out specimens with small thickness provide very limited resistance after peak load, while the pull-out specimens with large thickness provide relatively ductile failure due to the load is mainly born by the rebars. Thus, GFRP plate should be thick enough to avoid brittle failure from GFRP plates during in structural design.

5. Proposed strength equation

Push-out tests are an alternative method to determine the shear behavior of the plate connector. While, push-out test presented single shear crack failure pattern due to the combination of shear and bending [19]. Only for the failure modes from concrete dowel, those two different failure modes obtain similar results.

In this paper, strength prediction bases on the pull-out test. Two strength equations are adopted to consider different failure modes.

5.1. GFRP plate shear failure

From the preceding analysis, plate failure can be simplified as shear-out failure modes, similar to the mode of failure of GFRP bolted joints. Collings [24] proposed below equation to consider shear-out failure modes of bolted joints:

$$V_u = \tau_u e t \tag{1}$$

where e and t are end distance and plate thickness respectively, τ_u is the shear strength of GFRP laminations. While Eq. (1) is independent with the hole radius R of the plate, and is against the experimental data listed in Table 6. Hart [25] proposed a stress concentration factor K_{tc} to calculate the shear-out failure of GFRP laminations shown in Eqs. (2)–(4).

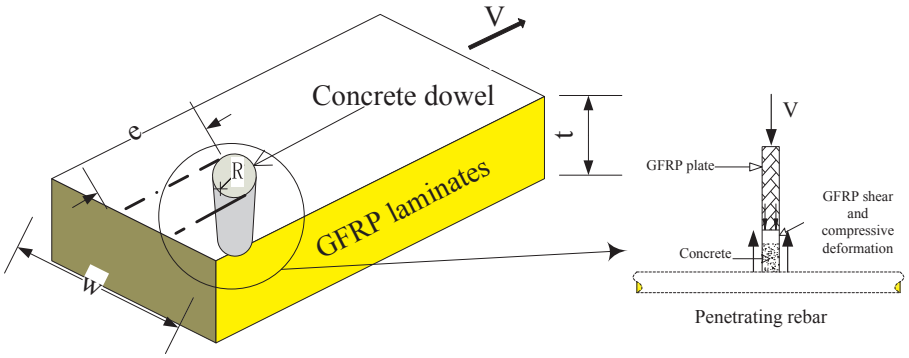

(a) GF specimen

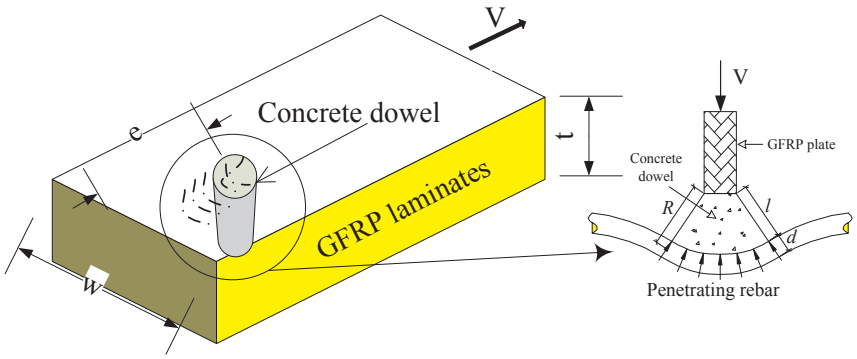

(b) CF specimen

Fig. 15. GPC failure mechanism.

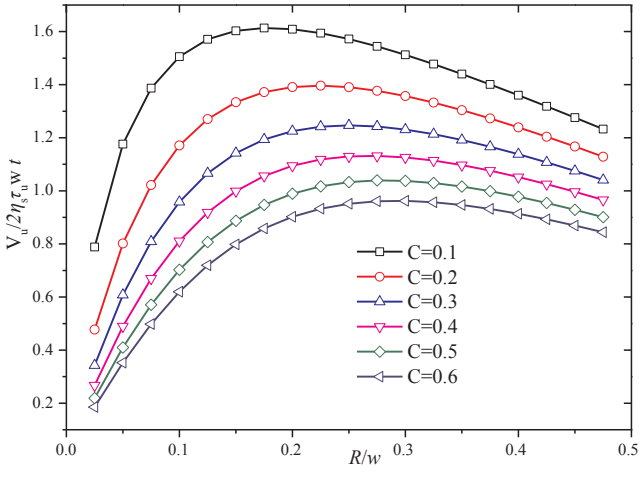

Fig. 16. Relationship between ultimate strength and ratio (R/w).

Table 7
Strength equations for concrete dowel failure.

References	Equation	Notation
Ge [26]	$V_u = 10.5n\pi f_t (d/2)^2 + A_s f_s$ (9)	n: number of holes f_t: concrete's tensile strength f_s: rebar's tensile strength h: the height of GPC t: the thickness of GPC
J.R. Cho [18]	$V_u = 5.77d^2\sqrt{f_c}$ (10)	
X. Zou [19]	$V_u = 4.5htf_c + 3.31nd^2\sqrt{f_c} + 0.91A_s f_s$ (11)	

Table 8
Concrete dowel failure data.

References	R (mm)	d_s (mm)	f_c (MPa)	V_u (kN)
author	20	16	50.9	222.9
	20	16	50.9	209.8
	25	16	50.9	239.8
	25	16	50.9	241.0
Nam	15	–	45.0	92.3
	15	–	45.0	86.9
J.R. Cho	12.5	–	58.1	27.3
	15	–	58.1	36.2
	17.5	–	58.1	53.0
	20	–	58.1	70.6
	20	–	58.1	81.1
	20	–	58.1	82.5
S. Zheng [16]	25	20	59.5	194.4
	30	20	59.5	213.1
	37.5	20	59.5	257.1
H. Huang [27]	17.5	–	31.3	75.9

$$K_{tc} = 1 + C(K_{te} - 1) \quad (2)$$

where C is a correlation factor for FRP bolted connection, it could be determined based on test results and the stress concentration of material with the same geometry. K_{te} is stress concentration factor, and could be determined by Eqs. (3) and (4).

$$K_{te} = \frac{w}{2R} - 1.5\frac{(w/2R - 1)}{(w/2R + 1)}\theta + 1 \quad (3)$$

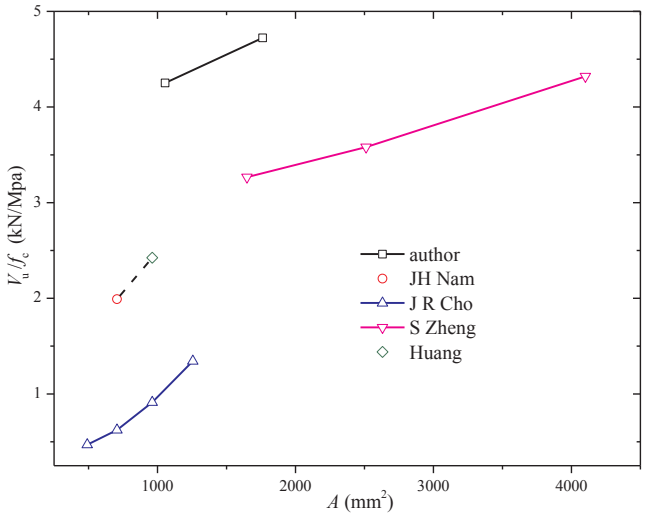

Fig. 17. Correlation between *A* and *Vu/fc*.

Table 9
Strength prediction comparison of concrete dowel failure.

Test	R	f_c	d_s	V_u	Eq. (9)/V_u	Eq. (10)/V_u	Eq. (13)/V_u
author	20	50.9	16	216.4	0.51	0.30	0.88
	25	50.9	16	240.4	0.55	0.43	1.01
J.R. Cho	12.5	58.1	–	27.3	0.64	1.01	1.20
	15			36.2	0.70	1.09	1.30
	17.5			53.0	0.65	1.02	1.21
	20			78.1	0.57	0.90	1.07
H. Huang	17.5	31.2	–	58.1	0.26	0.68	0.59

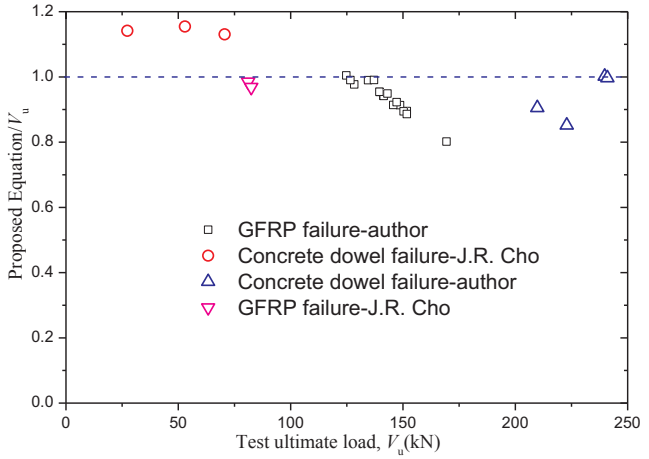

Fig. 18. Proposed equation validation.

$$\theta = \begin{cases} 1.5 - \frac{0.5}{e/w} & e/w \le 1 \\ 1.0 & e/w > 1 \end{cases} \quad (4)$$

where *w* is plate width. Related parameters are illustrated in Fig. 15. The plate shear failure strength equation is proposed by combing Eqs. (1) and (2), and expressed as Eq. (5). In addition, a coefficient η_s is introduced to consider material scatter. Then, the ultimate strength equation is expressed as Eq. (6).

The relationship between the strength and radius-to-width ratio (*R/w*) has been plotted in Fig. 16 by non-dimensional operating in Eq. (7). Through regression, $C = 0.15$, $\eta_s = 2.17$, is obtained. The ultimate strength of GPC under GFRP shear failure is given as Eq. (8).

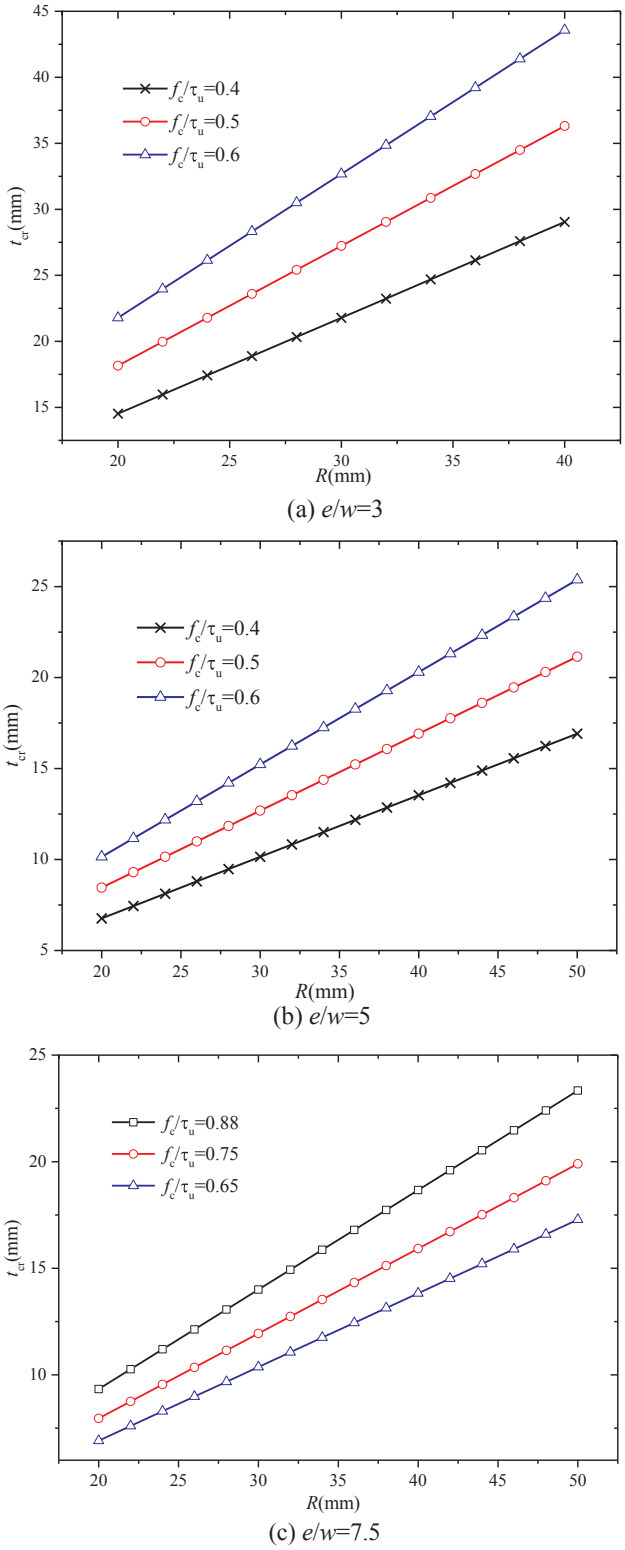

Fig. 19. Critical thickness under different dimensions.

$$V_u = \frac{2\tau_u(e-R)t}{K_{tc}} \quad (5)$$

$$V_u = \frac{2\eta_s\tau_u(e-R)t}{1 + C\left[\frac{w}{2R} - 1.5\frac{(w/2R-1)}{(w/2R+1)}\theta\right]} \quad (6)$$

$$\frac{V_u}{2\eta_s wt\tau_u} = \frac{(e-R)/w}{1 + C\left[\frac{w}{2R} - 1.5\frac{(w/2R-1)}{(w/2R+1)}\theta\right]} \tag{7}$$

$$V_u = \frac{4.34\tau_u(e-R)t}{1 + 0.15\left[\frac{w}{2R} - 1.5\frac{(w/2R-1)}{(w/2R+1)}\theta\right]} \tag{8}$$

5.2. Concrete dowel failure

The strength of GPC in terms of concrete dowel failure mode is dependent to following aspects: 1) concrete dowel action; 2) rebar's shear resistance; 3) the compression condition of the local plate; 4) concrete splitting resistance and 5) the adhesive action between the GFRP and concrete. Among these factors, the compression of the GFRP plate improves the local concrete strength in the compression area for confinement effects, and the adhesive action is complicated and susceptible to the treatment of the GFRP surface. Hence, the equation is founded by the omission of the 4th and 5th action. Equations to predict the strength of concrete dowel failure [18,19,26] are listed in Table 7. Based on the substantial test data in Table 8, the correlation between concrete dowel and hole area is obtained and plotted in Fig. 17. The ratio of V_u/f_c presented a linear trend with the area of the hole (A), the slope of which was fitted as 1.15. Then, the shear resistance could be expressed as Eq. (12).

$$V_u = 1.15Af_c \tag{12}$$

As regard to the concrete dowel with penetrating rebars, the restraint effect and shear resistance of rebar should be accounted for. With the derivation of Eq. (12), A is substituted by $(A - A_s)$. A_s is the area of penetrating rebar. A coefficient φ_{re} is introduced to consider the rebar's restraint action, Eq. (12) is rewritten as Eq. (13) with consideration of the penetrating rebar's effect.

$$V_u = 1.15\varphi_{re}(A - A_s)f_c + 1/\sqrt{3}A_s f_y \tag{13}$$

where φ_{re} is defined as $6.11\frac{d_s}{2R}$, d_s is the diameter of penetrating rebar.

5.3. Comparisons between equations and tests

The comparisons between different equations and experimental data are summarized in Table 9. The results show that the proposed equations in this paper have the minimum deviation. Tests carried out by Cho [18] including both GF and CF modes have also been used for the validation, and also shown in Fig. 18. A good agreement is observed.

5.4. Critical plate's thickness of GFRP plate

A critical plate thickness is defined as the limit between concrete dowel failure and GFRP shear failure. The expression of the critical plate thickness t_{cr} is shown as below based on the previous section:

$$t_{cr} = \frac{f_c}{\tau_u}\left[1.15\varphi_{re}(A - A_s) + 1/\sqrt{3}A_s\frac{f_y}{f_c}\right]\frac{1 + 0.15\left[\frac{w}{2R} - 1.5\frac{(w/2R-1)}{(w/2R+1)}\theta\right]}{4.34(e-R)} \tag{14}$$

The t_{cr} is dependent on concrete compression and laminate's shear strength. Given $w/2R = 3.25$, $d_s/2R = 0.32$, $f_y/f_c = 8.6$, $e/R = 3 \sim 7.5$, the critical plate thickness is shown in Fig. 19 in terms of different radius and f_c/τ_u. In the preliminary estimation during design, Fig. 19 provides a solution of the critical thickness to guarantee the sufficient strength and ductility of GPC.

6. Conclusions

Based on experimental results obtained from 26 tests and substantial theoretical analysis, the following conclusions related to the shear behaviors of pultruded GPC are drawn:

(1) The failure mode of GPC is determined by the larger item of shear resistance provided between the concrete dowel and GFRP shear modulus. Three stages could be classified from the measured load-slip curves including elastic stage, plastic stage and failure stage. $0.4V_u$ was observed as the turning point between the elastic stage and plastic stage. Secant of $0.4V_u$ has been proposed as the stiffness of GPC. Through the verification of the test data, $0.4V_u$ stiffness definition matched its mechanical meaning.
(2) When the specimens turn up GFRP shear-out failure: it usually occurs to the thin plate which has a relatively small shear bearing area. The plate hole radius took a significant effect on the ultimate strength. The penetrating rebar and type of rebar rarely affect the ultimate strength. GPC showed brittle characteristics when failure. In GFRP structural design, GFRP shear-out failure should be avoided. Concrete dowel failure has been usually accompanied by the compression damage of GFRP plate. When the specimens turn up concrete dowel failure: under the same plate's radius, its ultimate strength is larger than that of GFRP shear-out failure, especially with the presence of penetrating rebar such as R20d16D and R25d16D.
(3) Test data and other researcher's data have been gathered and fitted to make strength predictions on GPC. With respect to GFRP failure, stress concentration has been taken into account in the strength prediction. As regard to concrete failure, not only the penetrating rebar's shear resistance, but the restraint action on concrete brought by rebar has been involved in the strength equation. With a collection of other test data as complement, proposed strength equations (Eqs. (8) and (13)) for different failure mode have been verified to make a precise prediction of GPC's strength. To guarantee the rational strength and ductility of GPC, a critical thickness of the plate is proposed according to the strength equations. In the ultimate state, the critical thickness of the plate is located on the border between the concrete dowel failure and GFRP shear-out failure.

Acknowledgements

The authors gratefully acknowledge the financial supports by the NSFC project (No. 51578406 and 51808398) funded by National Natural Science Foundation of China, China Postdoctoral Science Foundation (No. 2018M642081).

References

[1] Bank LC. Composites for construction: structural design with FRP materials. New Jersey: John Wiley & Sons; 2006.
[2] Mosallam AS, Bayraktar A, Elmikawi M, et al. Polymer composites in construction: an overview. SOJ Mater Sci Eng 2015;2(1):25.
[3] Correia JR, Branco FA, Ferreira JG. Flexural behaviour of GFRP–concrete hybrid beams with interconnection slip. Compos Struct 2007;77(1):66–78.
[4] Xin H, Liu Y, Du A. Thermal analysis on composite girder with hybrid GFRP-concrete deck. Steel Compos Struct 2015;19(5):1221–36.
[5] Zuo Y, Mosallam A, Xin H, et al. Flexural performance of a hybrid GFRP-concrete bridge deck with composite T-shaped perforated rib connectors. Compos Struct 2018;194:263–78.
[6] Bank LC, Oliva MG, Bae HU, et al. Pultruded FRP plank as formwork and reinforcement for concrete members. Adv Struct Eng 2007;10(5):525–35.
[7] Keller T, Rothe J, De Castro J, et al. GFRP-balsa sandwich bridge deck: concept, design, and experimental validation. J Compos Constr 2013;18(2):04013043.
[8] Mastali M, Barros J, Valente I. Structural performance of hybrid sandwich slabs under shear loading. J Sandwich Struct Mater 2017. 1099636217699660.
[9] Xin H, Mosallam A, Liu Y, et al. Experimental and numerical investigation on in-plane compression and shear performance of a pultruded GFRP composite bridge deck. Compos Struct 2017;180:914–32.
[10] Xin H, Mosallam A, Liu Y, et al. Analytical and experimental evaluation of flexural behavior of FRP pultruded composite profiles for bridge deck structural design. Constr Build Mater 2017;150:123–49.
[11] Mosallam AS. Design guide for FRP composite connections, ASCE manuals and reports on engineering practice MOP (102). Reston, Virginia, USA: American

Society of Civil Engineers (ASCE); 2011. ISBN 978-0-7844-0612-0.
[12] Ascione F, Lamberti M, Razaqpur AG, et al. Strength and stiffness of adhesively bonded GFRP beam-column moment resisting connections. Compos Struct 2017;160:1248–57.
[13] Nguyen H, Mutsuyoshi H, Zatar W. Push-out tests for shear connections between UHPFRC slabs and FRP girder. Compos Struct 2014;118:528–47.
[14] El-Hacha R, Chen D. Behaviour of hybrid FRP–UHPC beams subjected to static flexural loading. Composites Part B 2012;43(2):582–93.
[15] Coelho AMG, Mottram JT. A review of the behaviour and analysis of bolted connections and joints in pultruded fibre reinforced polymers. Mater Des 2015;74:86–107.
[16] Zheng S, Liu Y, Yoda T, et al. Parametric study on shear capacity of circular-hole and long-hole perfobond shear connector. J Constr Steel Res 2016;117:64–80.
[17] Liu Y, Xiong Z, Feng Y, et al. Concrete-filled rectangular hollow section X joint with Perfobond Leister rib structural performance study: ultimate and fatigue experimental Investigation. Steel Compos Struct 2017;24(4):455–65.
[18] Cho JR, Park SY, Cho K, et al. Pull-out test and discrete spring model of fibre-reinforced polymer perfobond rib shear connector. Can J Civ Eng 2012;39(12):1311–20.
[19] Zou XX, Feng P, Wang JQ. Perforated FRP ribs for shear connecting of FRP-concrete hybrid beams/decks. Compos Struct 2016;152:267–76.
[20] Oguejiofor EC, Hosain MU. A parametric study of perfobond rib shear connectors. Can J Civ Eng 1994;21(4):614–25.
[21] Hosaka T, Mitsuki K, Hiragi H, et al. An experimental study on shear characteristics of perfobond strip and it's rational strength equations. J Struct Eng 2000;46:1593–604.
[22] Ministry of Construction of China. Code for design of concrete structure, GB50010-2010. Beijing, China: Communications Press; 2018. (in Chinese).
[23] Oehlers DJ, Coughlan CG. The shear stiffness of stud shear connections in composite beams. J Constr Steel Res 1986;6(4):273–84.
[24] Collings TA. On the bearing strength of CFRP laminates. Composites 1982;13(3):241–52.
[25] Hart-Smith LJ. Bolted joints in graphite-epoxy composites. MCDONNELL DOUGLAS CORP LONG BEACH CA DOUGLAS AIRCRAFT DIV; 1976.
[26] Chang Ge. Experimental and theoretical study on the static performance of FRP bridge deck. Shanghai, China: Tongji University; 2009. (in Chinese).
[27] Huang H, Li A, Chen L, et al. Push-out tests for shear connectors in GFRP-concrete composite bridge deck slabs. J Adv Concr Technol 2018;16(8):368–81.